Thermodynamic behavior in decaying, compressible turbulence with initially dominant temperature fluctuations

X. D. Cai, E. E. O'Brien, and F. Ladeinde
Department of Mechanical Engineering, State University of New York at Stony Brook, Stony Brook, New York 11794-2300

Direct numerical simulation of decaying, isotropic, compressible turbulence in three dimensions is used to examine the behavior of fluctuations in density, temperature and pressure when the initial conditions include temperature fluctuations larger than pressure fluctuations. The numerical procedure is described elsewhere, the initial turbulent Mach number is subsonic, 0.3 to 0.7, and the initial compressible turbulence is characterized as being in one of three states in which the ratios of initial kinetic energy in the compressible modes to total kinetic energy are, respectively, very small, moderate or nearly unity. Only at the lowest values of initial turbulent Mach number and energy ratio do thermodynamic scalings follow the predictions in the literature. For turbulent Mach numbers above 0.3, or for finite values of the kinetic energy ratio, the scalings are more complex. A relationship between turbulent Mach number, compressible pressure and energy ratio, which has been proposed previously for isothermal problems, appears to hold, on average, for the cases computed in this study, all of which are non-isothermal. © *1997 American Institute of Physics.* [S1070-6631(97)03106-1]

I. INTRODUCTION

In turbulent compressible flows the importance of pressure fluctuations, p, has received wide recognition in the literature. For example, with the aid of some simplifying assumptions about the molecular diffusion term such as Lewis number equal to one and the adoption of Fick's law, the conservation equation of energy in $(\mathbf{x}, \mathbf{t})$ space[1] can be written as

$$\frac{\partial}{\partial t}\rho h + \frac{\partial}{\partial x_k}\rho u_k h = \frac{\partial p}{\partial t} + \frac{\partial}{\partial x_k}\left(\frac{\mu}{P_r}\frac{\partial h}{\partial x_k}\right), \qquad (1)$$

where h is the static enthalpy per unit mass, ρ is density, u_k is a velocity component, μ is viscosity and P_r is the Prandtl number. The amplitude of $\partial p/\partial t$ determines whether the enthalpy can be usefully treated as a conservative variable, which is critical for non-premixed combustion theory. Pressure fluctuations, p, are also important in the modeling of compressible turbulence, especially terms such as pressure-dilatation,[2] $\langle pd \rangle$, where d is velocity divergence $\nabla \cdot \mathbf{u}$, and dilatational dissipation,[3] defined by $\epsilon_c = \frac{4}{3}\mu\langle d^2 \rangle$, where angular brackets denote an average. In low Mach number flows it has been generally believed that the pressure fluctuation is small compared to its mean, as in Morkovin's hypothesis.[4] Indeed, the well-known Sarkar *et al.* model[3] of ϵ_c inherently used this assumption.

Recently it was shown by Ghosh and Matthaeus,[5] in their direct simulations of turbulent polytropic flow in two dimensions, that there exist three distinct types of turbulence, even for low Mach number flow. They cataloged them as (a) nearly incompressible flows dominated by vorticity, (b) flows characterized by near statistical equipartition of energy in vortical and compressive modes and (c) nearly pure acoustic turbulence dominated by compressive modes. The distinctly different scalings of density fluctuations associated with each of these flow types suggest that the pressure fluctuations might also have distinctly different behavior in each of these flows.

This concept is strengthened by the results of Sarkar *et al.*[3] which show that the compressible part of pressure is well correlated with both the fraction of kinetic energy associated with the compressible modes, say χ, as well as with the turbulent Mach number M_t, which is defined as rms velocity divided by the average speed of sound. Passot and Pouquet[6] demonstrated the strong role of M_t in earlier two-dimensional calculations. A question arises as to how this more complex pressure behavior affects the relationships between density, pressure and temperature when the phenomenon of heat transfer *via* large initial variation in temperature with position is added to the problem. Zank and Matthaeus[7,8] and Bayly, Levermore and Passot[9] found, for nearly incompressible flows, case (a), that evolution of the behaviors of these three thermodynamic variables depended on the relative magnitudes of their initial rms values. Zank and Matthaeus considered two cases, one in which initial temperature fluctuations were of the same order as pressure fluctuations, and the other in which initial temperature fluctuations were much larger than the initial pressure fluctuations. In the latter case they showed that the density and temperature fluctuations become anti-correlated as the flow evolves. They proposed that their predictions may apply more widely than to just the nearly incompressible situation.

One purpose of this study is to check the Zank's and Matthaeus' scaling predictions[7,8] for each of the three types of compressible turbulence mentioned above. This study can also be considered as an extension of the seminal work of Ghosh and Matthaeus[5] by further elucidating the nature of compressible subsonic turbulence in three dimensions with heat transfer. In the next section we discuss in more detail the theoretical and analytical background of this research. In Sec. III we present the numerical method and list the types of

initial conditions from which our simulations run. The simulation results and there limitations are discussed in Sec. IV, and are compared with the predictions of Sec. II. In the final section we summarize the results.

II. THEORETICAL BACKGROUND

In the literature of compressible turbulence the viscous terms in the energy equation are often neglected since the effect of viscosity is felt either on a viscous time scale (much greater than the acoustic time scale) or during the formation of shocks which are scarce in flows in which the Mach number is well below unity. In an analysis which excluded viscous effects, Zank and Matthaeus[8] used the nearly incompressible (NI) hydrodynamic theory of Klainerman and Majda[10] to study thermodynamic scalings in decaying compressible turbulence[11] when independent initial temperature fluctuations and the process of heat conduction are included in the energy equation for NI turbulence. The central issue of their theory was to seek the specific orders of magnitude of temperature, pressure and velocity fluctuations which are needed to obtain the solutions to the incompressible dynamical equations as the first order solution of the compressible equations in an asymptotic expansion in sonic Mach number M_s as the small parameter. M_s is defined as a characteristic velocity divided by the average speed of sound; $M_s = M_t$, the turbulent Mach number, when the rms velocity is chosen as the characteristic velocity. If the initial temperature fluctuations, T', are of order M_s, which is larger than the pressure fluctuations, $p', p' = \bigcirc(M_s^2)$, and if the compressible fraction of kinetic energy, χ, is also small, $\chi = \bigcirc(M_s^2)$, then, they found, density fluctuations are anti-correlated with temperature fluctuations. That is, $\rho' = -T'$. Here, and throughout the remainder of this paper, a prime ($'$) will indicate a fluctuation about a mean value.

This result can be formally understood from the equation of state. For an ideal gas, when the mean pressure, density and temperature are each normalized to unity, and if the fluctuations about these means are small enough, then, approximately,

$$p' = T' + \rho'. \qquad (2)$$

If $\rho' = \bigcirc(M_s)$ and if p' maintains a magnitude of order M_s^2 throughout the evolution of the flow, then ρ' and T' will be anti-correlated and T' will be of order M_s.

The behavior of pressure fluctuations, p', has been predicted by Sarkar et al.[3] without consideration of heat conduction in the energy equation. They made use of an asymptotic method of Erlebacher et al.,[12] in which the original problem is reduced to several simpler sets of equations by decomposing the dependent variables into one set which solves a known problem, and a second set which satisfies a new evolution equation. In this theory, the velocity is split into an incompressible, solenoidal velocity, u_i^I, and a compressible velocity, u_i^C, and the corresponding pressure is changed into an incompressible pressure p^I and a compressible pressure p^C, where u_i^I, p^I satisfy the incompressible equations, and u_i^C, p^C satisfy the wave equation on the acoustic time scale t_c.

Since p^I satisfies a Poisson equation for incompressible pressure, it retains the order of M_s^2 as the flow evolves. Meanwhile p'^C is shown to satisfy the following relationship:

$$F = \frac{\gamma^2 M_t^2 \chi}{\langle (p'^C)^2 \rangle} \simeq 1, \qquad (3)$$

where M_t is the turbulent Mach number, γ is the polytropic index and χ is the ratio of turbulent kinetic energy in the compressible modes to the total turbulent kinetic energy, $\chi = \langle u_i^C u_i^C \rangle / (\langle u_i^C u_i^C \rangle + \langle u_i^I u_i^I \rangle)$. The turbulent Mach number M_t is defined by $M_t = u_{rms}^* / c^*$, where u_{rms}^* is given by $\langle u_i^* u_i^* \rangle^{1/2}$ and c^* is the average sound speed: $c^* = \langle (\gamma R^* T^*)^{1/2} \rangle$. The angle bracket denotes a space average or, in these statistically homogeneous computations, an ensemble average.

Equation (3) implies that, at acoustic equilibrium, there is an approximate equipartition between the kinetic and potential components of the compressible energy. It predicts that the compressible pressure fluctuations will depend strongly on χ, aside from any direct Mach number effect. In particular it means that the pressure may rise to be of order M_t when χ is of order 1. From the numerical simulations of Ghosh and Matthaeus,[5] we know that the nature of low Mach number flow depends strongly on the initial value of χ, say χ_0. For $\chi_0 \simeq 0$, low Mach number flows always remain nearly incompressible. That is, $\chi = \bigcirc(M_t^2)$. In this case, $p'^C = \bigcirc(M_t^2)$, which is of the same order as p'^I. Thus the total pressure is of order M_t^2, which further implies that the Zank and Matthaeus anti-correlation between ρ' and T' is recovered when either of them is of order M_t.

In the light of (3) it is also possible to predict a breakdown of the theory developed by Zank and Matthaeus[8] when the initial velocity consists mainly of longitudinal modes, $\chi_0 \simeq 1$. Then the pressure fluctuations are of order M_t and the anti-correlation between ρ' and T' is lost. Further, we note that (3) was obtained for cases in which heat conduction is neglected. The question then arises as to whether (3) remains valid when temperature fluctuations are dominant over pressure fluctuations initially. From the full energy equation it is easy to show that the effects of heat conductivity on the evolution of pressure fluctuations are indeed negligible on the acoustic time scale, which validates our use of the scaling relationships in the results presented in the above analysis. Numerical results reported in Sec. IV support this conclusion.

III. EQUATIONS AND NUMERICAL METHOD

The time-dependent compressible Navier–Stokes equations are solved in non-dimensional form. In order for it to be compatible with the ENO (essentially non-oscillatory) code developed by Shu et al.,[13] the velocity scale is chosen to be u_0^*, the speed of sound divided by the square root of the ratios of specific heats, that is, $u_0^* = (R^* T_0^*)$, where R^* is the specific gas constant and T_0^* is the initial mean temperature. Denoting the velocity field by u_i^*, we define the non-dimensional velocity, $u_i = u_i^* / u_0^*$. Since the mean flow field in homogeneous turbulence has no intrinsic length

scale, we choose turbulent integral length scale, L_0^*, which is defined as in incompressible turbulence,[14] as the reference length. The non-dimensional spatial coordinate is therefore $x_i = x_i^*/L_0^*$, and time is non-dimensionalized as $t = t^* u_0^*/L_0^*$. The density is scaled by the initial mean density, ρ_0^*, so that $\rho = \rho^*/\rho_0^*$. For consistency, the temperature, T, pressure, p and energy per unit mass are non-dimensionalized by, respectively, the initial mean temperature, T_0^*, the initial mean pressure, p_0^*, where $p_0^* = \rho_0^* R^* T_0^*$ and the mean square velocity $|u_0^*|^2$. The viscosity is non-dimensionalized as $\mu = 1/\mathrm{Re}_r = \mu^*/\rho_0^* u_0^* L_0^*$, μ^* is assumed constant and Re_r is the reference Reynolds number. The Prandtl number, $P_r = \mu^* C_p^*/\sigma^*$, where σ^* is the thermal conductivity and C_p^*, the specific heat, is also constant. In all the above definitions the superscript (*) denotes a dimensional variable.

With the above non-dimensionalization, the compressible Navier–Stokes equations can be written as

$$\frac{\partial \rho}{\partial t} + \frac{\partial}{\partial x_i}(\rho u_i) = 0, \tag{4}$$

$$\frac{\partial}{\partial t}(\rho u_i) + \frac{\partial}{\partial x_j}(\rho u_i u_j)$$
$$= -\frac{\partial p}{\partial x_i} + \frac{\partial}{\partial x_j}\left[\mu\left(\frac{\partial u_i}{\partial x_j} + \frac{\partial u_j}{\partial x_i} - \frac{2}{3}\frac{\partial u_k}{\partial x_k}\delta_{ij}\right)\right], \tag{5}$$

$$\frac{\partial}{\partial t}(\rho e_T) + \frac{\partial}{\partial x_j}(\rho e_T u_j)$$
$$= \frac{\partial}{\partial x_i}\left[-p\,\delta_{ij}u_j + \mu\left(\frac{\partial u_i}{\partial x_j} + \frac{\partial u_j}{\partial x_i} - \frac{2}{3}\frac{\partial u_k}{\partial x_k}\delta_{ij}\right)u_j \right.$$
$$\left. + \frac{\mu}{(\gamma-1)P_r}\frac{\partial T}{\partial x_i}\right], \tag{6}$$

where e_T is the non-dimensional total energy given by $e_T = e + \frac{1}{2}u_j u_j$, e is the non-dimensional internal energy and the second coefficient of viscosity, λ, is taken as $\lambda = -\frac{2}{3}\mu$. In this system the equation of state becomes $p = \rho T$. Equations (4), (5) and (6) are solved by time advancement in a periodic box. The high order spatial integration required for DNS is obtained here via the ENO procedure[13] and a third-order Runge–Kutta TVD method[13] is used for time integration. The efficiency and accuracy of this ENO scheme has been assessed by Ladeinde et al.[15,16]

TABLE I. Initial conditions for temperature, pressure and density fluctuations.

Variable	Initial conditions
Pressure	$p_0' = p_0'^c + p_0'^I$, where $p_0'^I$ satisfies Poisson equation $\nabla^2 p_0'^I = -\nabla \cdot (\mathbf{u}^I \cdot \nabla \mathbf{u}^I)$, and $p_0'^c = -p_0'^I$.
Temperature	$T_0' = \sqrt{|p_0'^I|} \cdot \mathrm{sgn}(p_0'^I)$, where sgn is the sign function
Density	$\rho_0' = \dfrac{1}{1+T_0'} - 1$

The connection between initial velocity and thermodynamic state data, and the occurrence of any of the flow regimes described in the Introduction have been elucidated by Ghosh and Matthaeus[5] and Zank and Matthaeus.[8] In order to specify the order of magnitude of the fluctuation of the various thermodynamic variables, we impose an initial pressure fluctuation field, p_0^I, computed from the incompressible pressure Poisson equation obtained from (5). That is,

$$\nabla^2(p_0'^I) = -\nabla \cdot (\mathbf{u}^I \cdot \nabla \mathbf{u}^I).$$

Then we set the initial total fluctuation pressure p_0' to zero so that its compressible component $p_0'^C$ satisfies $p_0'^C = -p_0'^I$, $p_0'^I$ is of order M_t^2 initially and, to obtain an initial temperature fluctuation field, T_0', of order M_t, we adopt the relationship $T_0' = \sqrt{|p_0'^I|} \cdot \mathrm{sgn}(p_0'^I)$, where sgn is a sign function. The corresponding initial density fluctuation field is obtained from

$$\rho_0' = \frac{p_0}{T_0} - 1 = \frac{-T_0'}{1+T_0'}.$$

With this prescription we arrive at a situation in which the temperature fluctuations are initially much larger than the pressure fluctuations, a condition required for validity of the low Mach number scaling theory of Zank and Matthaeus.[8] A summary of these initial conditions on the fluctuation of thermodynamic quantities is presented in Table I. In order to determine the separate effects of Mach number and compressible energy fraction χ on (3), and on the evolution of the scales of fluctuations in density, pressure and temperature, we adopt the procedure of Ladeinde et al.,[15] noting that different values of χ can be obtained through a different weighting of the compressible component in spectral space.

In Table II, columns 2 and 3, we have listed the initial

TABLE II. List of run Cases, initial values of parameters χ_0 and M_{t0} and values of parameters χ and M_t and correlation coefficients R_p, $C_{\rho T}$ and $C_{\rho p}$ at $t = 2.5$.

| Run case	χ_0	M_{t0}	$\chi(t=2.5)$	$M_t(t=2.5)$	$R_p(t=2.5)$	$C_{\rho T}(t=2.5)$	$C_{\rho p}(t=2.5)$
SVHD1	0	0.3	0.0079	0.17	5.79×10^{-1}	-0.93	0.29
SVHD2	0	0.5	0.027	0.28	6.10×10^{-1}	-0.58	0.61
RVHD1	0.6	0.3	0.34	0.12	4.04×10^{-2}	-0.34	0.70
RVHD2	0.6	0.5	0.30	0.21	7.41×10^{-2}	0.099	0.85
RVHD3	0.6	0.7	0.29	0.30	1.07×10^{-1}	0.27	0.91
LVHD1	1.	0.3	0.94	0.083	1.72×10^{-3}	-0.45	0.65
LVHD2	1.	0.5	0.88	0.14	5.40×10^{-3}	-0.18	0.77
LVHD3	1.	0.7	0.83	0.19	3.54×10^{-2}	0.059	0.87
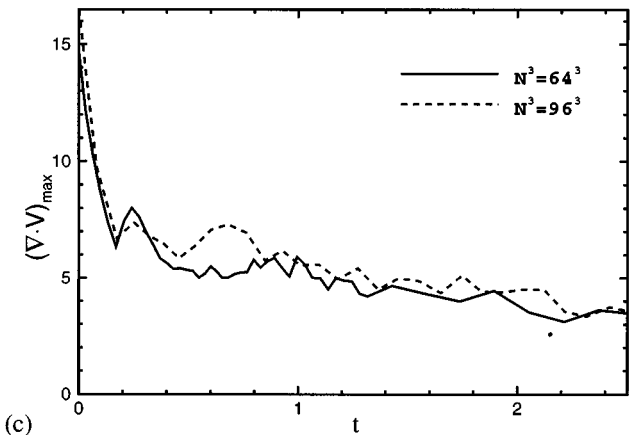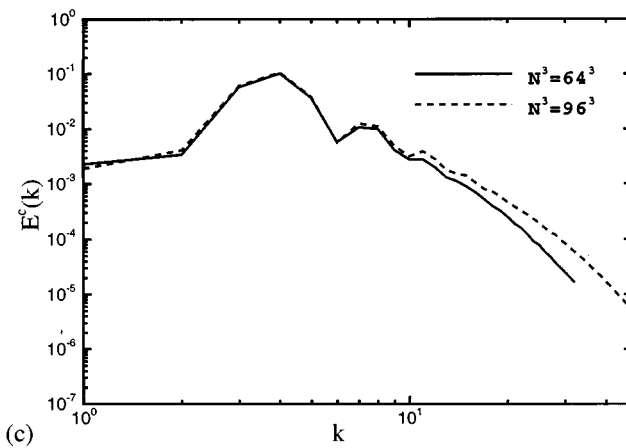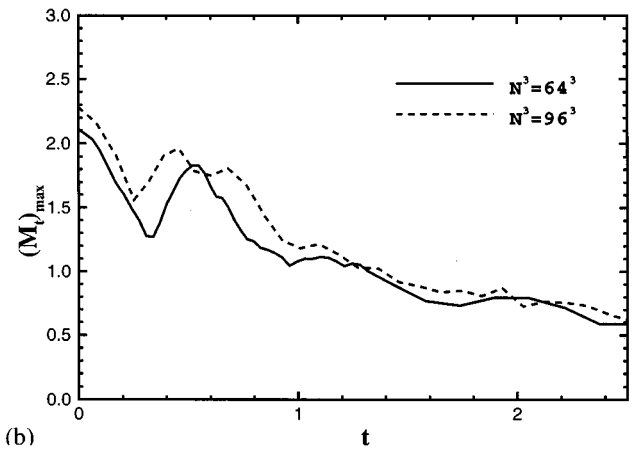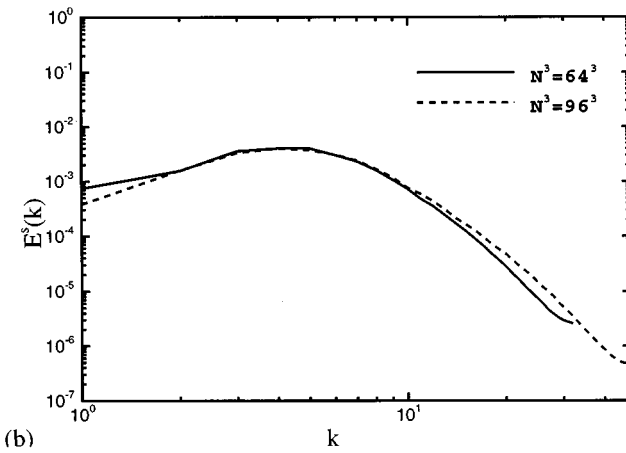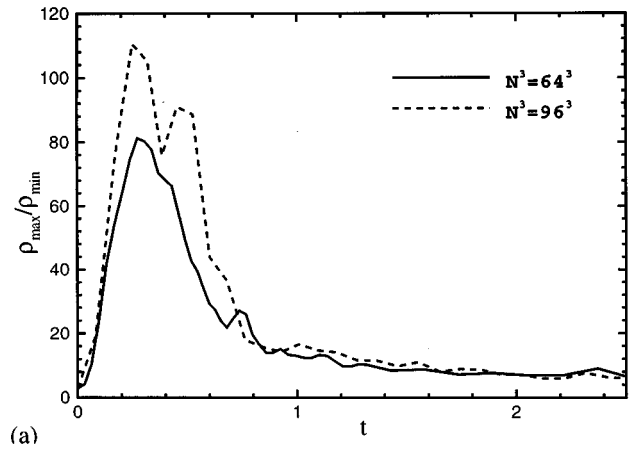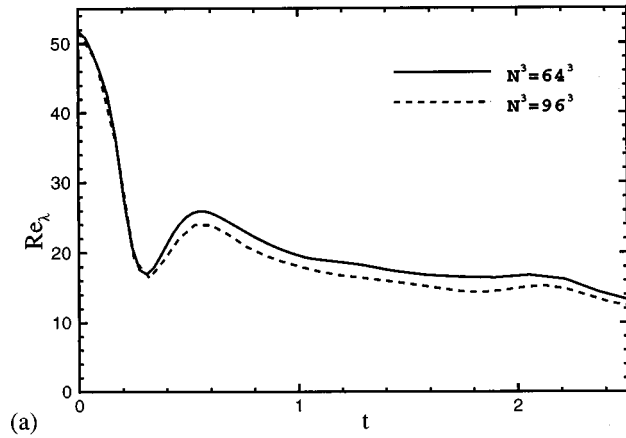
FIG. 1. Comparison between coarse mesh ($N^3 = 64^3$) and fine mesh ($N^3 = 96^3$) in case LVHD3: (a) time evolution of Taylor scale Reynolds number Re_λ; (b) incompressible energy spectrum $E^s(k)$ at $t=0.6$; (c) compressible energy spectrum $E^c(k)$ at $t=0.6$.

FIG. 2. Comparison of time evolution between coarse mesh ($N^3 = 64^3$) and fine mesh ($N^3 = 96^3$) in case LVHD3: (a) local density ratio ρ_{max}/ρ_{min}; (b) local maximum turbulent Mach number $(M_t)_{max}$; (c) local maximum velocity divergence $(\nabla \cdot \mathbf{V})_{max}$.

values of turbulent Mach number, M_{t0}, and compressible energy fraction, χ_0, for 8 computational runs, which use the initial prescriptions described in the previous paragraph. These encompass the approximate values $M_{t0}=0.3$, 0.5 and 0.7 and $\chi_0=0$, 0.6 and 1.0. Two other cases featuring slightly different initial conditions have been computed and are discussed in Sec. IV in the context of numerical results

obtained for the runs listed in Table II. The significance of the initials assigned to each run, such as SVHD, is as follows.

SV signifies a nearly incompressible, mostly solenoidal velocity field with the fraction of energy in the compressible modes close to 0. RV (random velocity) signifies an approxi-
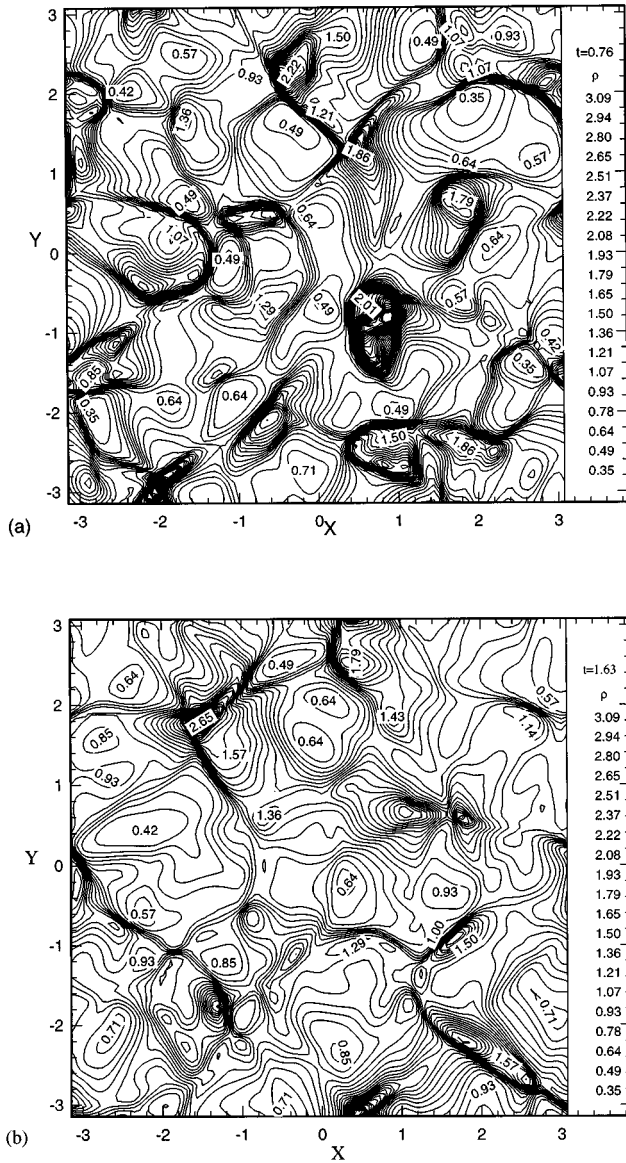
FIG. 3. Density contours for case LVHD3 with 96^3 mesh at (a) $t=0.76$ and (b) $t=1.63$.

mate balance between energies in the solenoidal and compressible modes. In our RV cases the associated values of χ_0 are in the neighborhood of 0.6, so that 60% of the kinetic energy is in the compressible modes, initially. LV (longitudinal velocity) designates cases in which the initial velocity field consists almost entirely of longitudinal modes with negligible vorticity; χ_0 is approximately 1. The methods used to generate these compressible velocity fields are described in detail in Ladeinde *et al.*[15] The letters HD stand for heat dominated,[8] which is common to all the simulation runs in this study.

In most of the computational cases the grid size is 64^3, the Prandtl number is set at $P_r=0.7$, the reference Reynolds number, $\mathrm{Re}_r = \rho^* u_0^* L_0^* / \mu^*$, at 200 and the energy spectrum has the form

$$E(k) \sim k^4 \exp(-k^2/2k_0^2), \qquad k_0=4.$$

It is well known that, to fully resolve the flow scales, we require that

$$k_{\max}\eta \gtrsim 1.0,$$

where η is the Kolmogorov length scale and $k_{\max}$ is the maximal resolved wave number. For the spectral method, $k_{\max} \simeq 30.17$ for 64^3. Based on the results in Ladeinde *et al.*,[15] we assume this estimation of $k_{\max}$ is applicable in our numerical method. Thus, under the conditions of our simulations [$\mathrm{Re}_r=200$, $(M_t)_{\max}=0.7$], $k_{\max}\eta$ can be estimated as larger than 0.98 initially, which suggests that the smallest characteristic flow scales are resolved in our calculations. At the same time, the domain size of 2π, which is normalized by the integral length scale, L_0^*, ensures that the periodic boundary conditions will not unduly constrain the solution. Using a procedure described elsewhere,[15] we are able to set the initial value of Mach number, M_{t0}, independently to begin the computation. The values of initial compressible energy fraction, χ_0, are obtained by exploiting the three different types of compressible turbulence promulgated by Ghosh and Matthaeus,[5] as mentioned in the Introduction.

In Sec. IV the results of these simulations are plotted as an evolution over time from the initial states described above. The non-dimensional time, t, is defined by $t=t^*/\tau_{e0}^*$, where τ_{e0}^* is the eddy turn-over time at $t=0$. τ_e^*, the eddy turn-over time, is defined by λ^*/u_{rms}^*, where λ^* is the Taylor microscale of the flow.

IV. NUMERICAL RESULTS

The computer resources available for these 3-D simulations generally limited us to a 64^3 mesh, with the possibility of some 96^3 mesh calculations to investigate whether there was adequate resolution to obtain the scaling laws of the more compressible LVHD cases. Porter, Pouquet and Woodward[17] have reported a numerical simulation of decaying supersonic turbulence on a 512^3 computational mesh, but without initially dominant temperature fluctuations.

The scaling laws for rms pressure, density and temperature are expected to be mostly sensitive to the energy containing regions of the spectra and may not be particularly sensitive to the small scale structure, which is the first to suffer from inadequate resolution. To test this concept we computed, at both 64^3 and 96^3 resolutions, the evolution in time of the Taylor-scale Reynolds number, Re_λ, defined as

$$\mathrm{Re}_\lambda = \left(\frac{5}{3\mu\varepsilon}\right)^{1/2} \langle\rho\rangle\langle|\mathbf{u}|^2\rangle,$$

where ε is the energy dissipation rate, and the compressible and incompressible energy spectra,[17,18] for two cases SVHD1 and LVHD3, respectively: the least and most compressible cases. Figure 1 shows the results for LVHD3. The initial conditions are nearly identical, but it is clear that there is a resolution problem at the highest wave numbers in this case. In the SVHD1 case (not shown), the simulation results for Re_λ and the energy spectra at 64^3 and 96^3 are virtually indistinguishable except at the far tail of the compressible energy spectrum where the energy level is negligible.

Cai, O'Brien, and Ladeinde
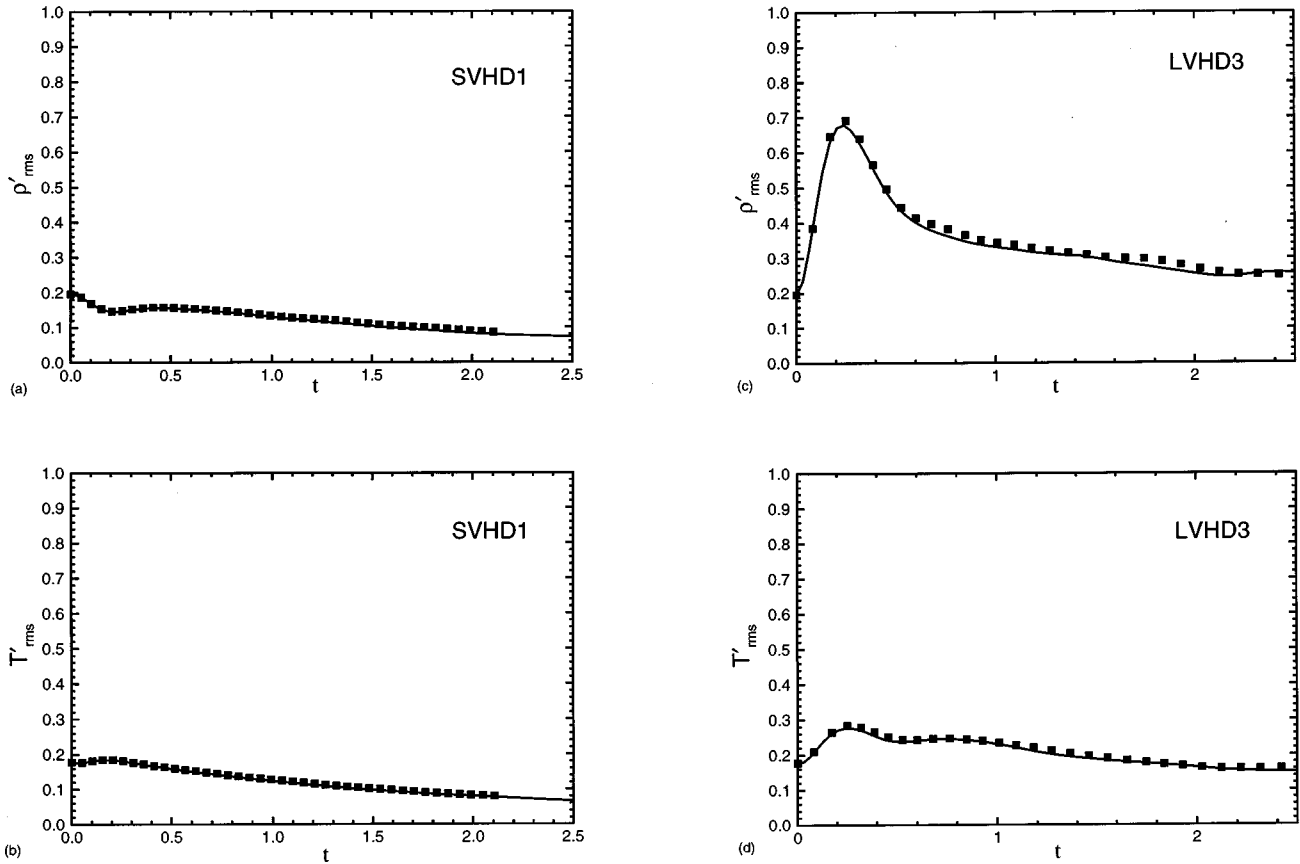
FIG. 4. Comparation of time evolution between coarse mesh ($N^3 = 64^3$, solid line) and fine mesh ($N^3 = 96^3$, solid square symbol): (a) rms density ρ'_{rms} in case SVHD1; (b) rms temperature T'_{rms} in case SVHD1; (c) rms density ρ'_{rms} in case LVHD3; (d) rms temperature T'_{rms} in case LVHD3.

In Figs. 2(a), 2(b) and 2(c), other aspects of the resolution problem are shown for the LVHD3 case; the SVHD1 case (not shown), which is nearly incompressible, displays virtually no difference between 64^3 and 96^3 simulations. Although there are significant discrepancies in the local density ratio, ρ_{max}/ρ_{min} and the local maximum values of Mach number and velocity divergence, they are predominantly in the early stages of the decay and may be partially due to differences in initial conditions. As the flow evolves from its highly compressible initial state these parameters tend toward the same asymptotic state independent of mesh size.

In Fig. 3, we show two typical density contours for the LVHD3 case at $t=0.76$ [Fig. 3(a)] and $t=1.63$ [Fig. 3(b)] with 96^3 mesh size. These are times at which the local turbulent Mach number is, respectively, supersonic and subsonic as shown in Fig. 2(b). The density gap between contours is the same ($\delta\rho \simeq 0.072$) in both cases. The prevalence of much steeper density gradient regions at the earlier time may be an indication that the resolution is at least capable of locating the presence of local supersonic regions in the flow. At the same density gap no such steep gradient regions occur in the SVHD1 case (not shown). At 64^3 mesh and $t=0.63$, the LVHD3 case also displays regions of high density gradient, but with less intensity than the 96^3 simulation at the same gap between contours (not shown).

In Fig. 4, the scaling behaviors of both density and temperature fluctuations are displayed for the SVHD1 and LVHD3 cases for both 64^3 and 96^3 meshes. The SVHD1 case [Fig. 4(a) and Fig. 4(b)] is unaffected by increased mesh size as expected, and the highly compressible LVHD3 case [Fig. 4(c) and Fig. 4(d)] shows very little effect of the resolution imprecision seen in the earlier figures. The resolution at 64^3 appears to be adequate for our purpose, which is to determine scaling laws.

The quantity F defined by (3) was computed for all eight runs listed in Table II, as well as for two other runs not appearing there. Surprisingly, except for a brief initial transient, the average value, $\langle F \rangle$, was close to unity for all runs, although (3) was derived from an asymptotic theory[12] in the absence of heat conduction.[3] As a consequence, the compressible pressure fluctuations are independently tied, apparently, to both turbulent Mach number and energy ratio, at least on the average, whether the flow energy is mostly in the compressible or solenoidal modes. In Fig. 5 we display F versus t for two cases SVHD1, in which both χ_0 and M_{t0} are small, and LVHD2, in which they are larger. All other runs produced similar results for F, which oscillates about 1 with amplitudes and periods increasing slightly as the magnitudes of χ_0 and M_{t0} increase.

In Figs. 6–8 we show the evolutions of rms density, ρ'_{rms}, temperature, T'_{rms}, and pressure, p'_{rms}, for each of the eight runs. To each of these figures, except the first, we have added $\gamma\rho'_{rms}$ to indicate how far the thermodynamic state is
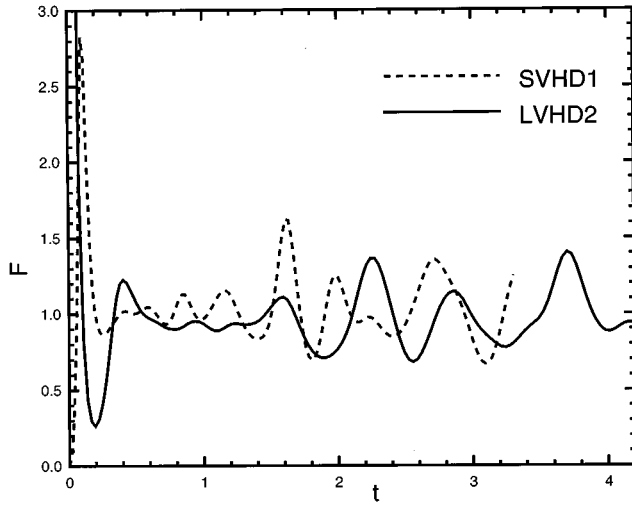
FIG. 5. Time evolution of parameter F, $F = \gamma^2 M_t^2 \chi / \langle p'^C \rangle^2$. ---, SVHD1 ($\chi_0=0$, $M_{t0}=0.3$);—, LVHD2 ($\chi_0=1$, $M_{t0}=0.5$).

from an asymptotic acoustic limit in which $p' = \gamma \rho'$. In each figure, a brief initial transient is evident in the evolution. It is caused by our choice of initial conditions which are chosen to conform to NI theory. Our interest is in the thermodynamic behaviors beyond the transients which last for at most $0.5\tau_{e0}^*$ and which we ignore in the following discussion. One general observation from these figures is the decrease in the rate of decay of T'_{rms} as initial Mach number M_{t0}, or initial energy ratio χ_0, is increased.

The results of case SVHD1 are plotted in Fig. 6(a). This case is the closest to the NI limit in which the prediction $\rho'_{rms} = T'_{rms}$ is expected to be realized. Figure 6(a) shows that it is, approximately, and that pressure fluctuations are significantly less than those of density and temperature. Case SVHD2, presented in Fig. 6(b), like SVHD1, is almost totally solenoidal initially, but begins with a higher initial Mach number than SVHD1. In this case the density fluctuations grow to be larger than the temperature fluctuations, which are comparable in magnitude to the pressure fluctuations, $T'_{rms} \simeq p'_{rms} < \rho'_{rms}$. Although ρ'_{rms} is only moderately larger than T'_{rms} it is clear that the predictions of Zank and Matthaeus[8] for NI turbulence that they are equal does not carry accurately up to $M_{t0}=0.5$.

Figure 7 shows results for the RVHD cases, which are initially in a state of approximate equipartition of energy between compressible and solenoidal modes, $\chi_0=0.6$. The case with the lowest M_{t0} is RVHD1, and the results of this simulation are presented in Fig. 7(a). In this case we find $T'_{rms} < \rho'_{rms} \simeq p'_{rms}$. The higher χ_0 has enhanced the magnitude of pressure fluctuations significantly, and the density fluctuations somewhat, compared to those from SVHD1 [Fig. 6(a)] which has the same $M_{t0}=0.3$. Figure 7(b) gives the results for RVHD2, which differs from RVHD1 by an increase in M_{t0} from 0.3 to 0.5. In this case, $T'_{rms} < \rho'_{rms} < p'_{rms} < \gamma \rho'_{rms}$, which indicates an increase in pressure fluctuation intensity with Mach number, relative to the intensities of temperature and density fluctuations. When the Mach number is increased further to $M_{t0}=0.7$, the

RVHD3 case, it can be seen from Fig. 7(c) that the pressure fluctuation amplitude almost reaches the acoustic limit in which $p'_{rms} = \gamma \rho'_{rms}$.

The three cases in which the initial state of the turbulence consists almost entirely of compressive modes are LVHD1, 2 and 3. In Fig. 8(a), the rms thermodynamic quantities for LVHD1 show a remarkable similarity to the low Mach number ($M_{t0}=0.3$) RVHD1 case. The existence of a larger fraction of compressible modes in the former case does not seem to have a strong effect on the relative sizes of the thermodynamic fluctuations, although it does enhance their amplitudes. Again, $T'_{rms} < \rho'_{rms} \simeq p'_{rms}$. It should be noted that this is not the behavior of SVHD1 [$p'_{rms} < T'_{rms} \simeq \rho'_{rms}$, Fig. 6(a)] which is also at $M_{t0}=0.3$, but is of a different character, being nearly incompressible.

When M_{t0} is increased to $M_{t0}=0.5$ [case LVHD2, Fig. 8(b)] we find a similar situation. The relative behaviors of T'_{rms}, ρ'_{rms} and p'_{rms} are qualitatively like those seen in Fig. 7(b), case RVHD2, which has the same initial Mach number. That is, $T'_{rms} < \rho'_{rms} < p'_{rms} < \gamma \rho'_{rms}$. However, the magnitudes of these fluctuations are increased in the LVHD2 case by as much as 15% over those of RVHD2. At the higher initial Mach number, $M_{t0}=0.7$, which is presented in Fig.


(a)

(b)
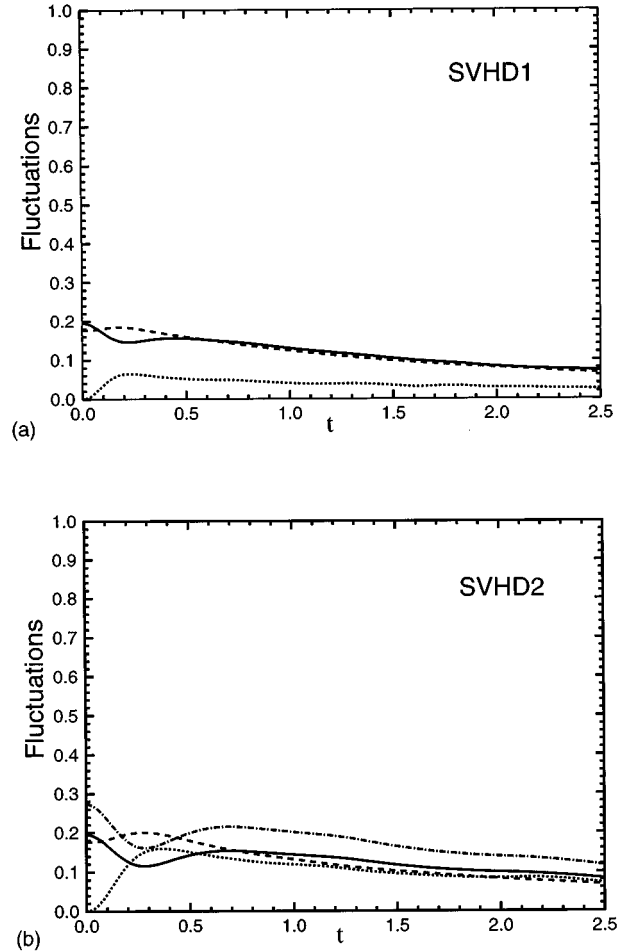
FIG. 6. Time evolution of rms density, ρ'_{rms}, temperature, T'_{rms}, pressure, p'_{rms} and $\gamma \rho'_{rms}$ in (a) case SVHD1 ($\chi_0=0$, $M_{t0}=0.3$); (b) case SVHD2 ($\chi_0=0$, $M_{t0}=0.5$):—, ρ'_{rms}; ---, T'_{rms}; $\cdots$, p'_{rms}; -·-, $\gamma \rho'_{rms}$.
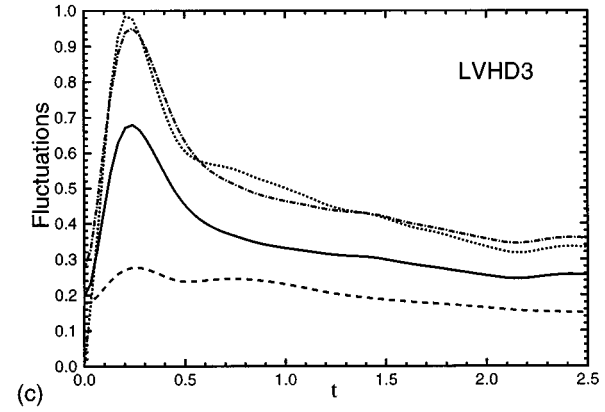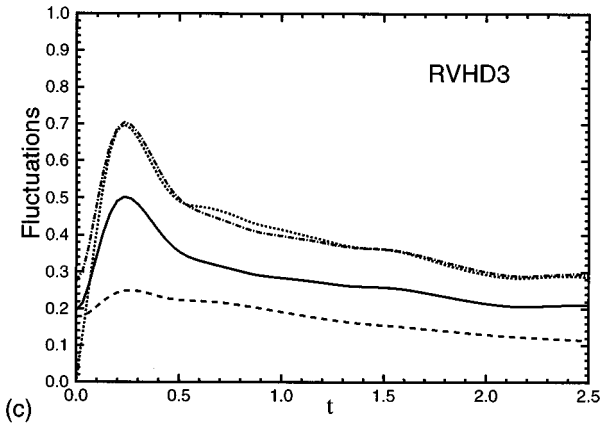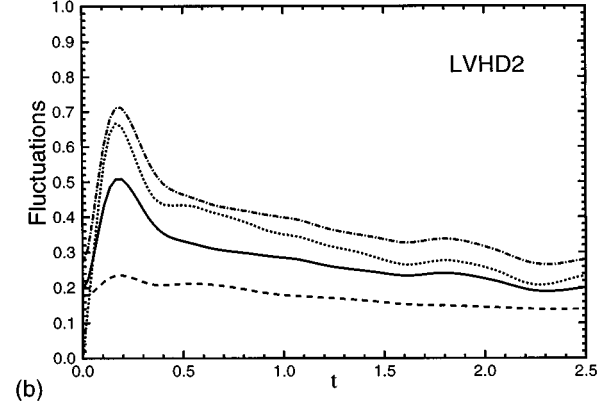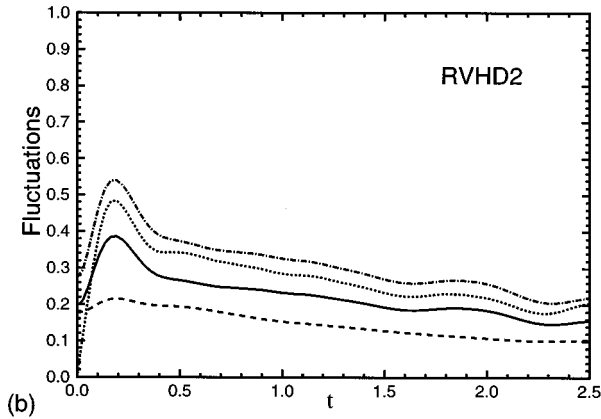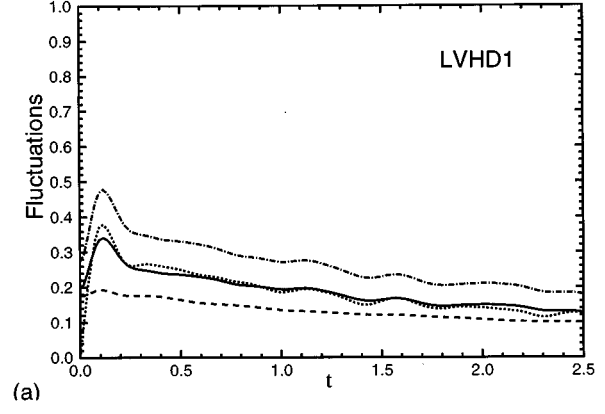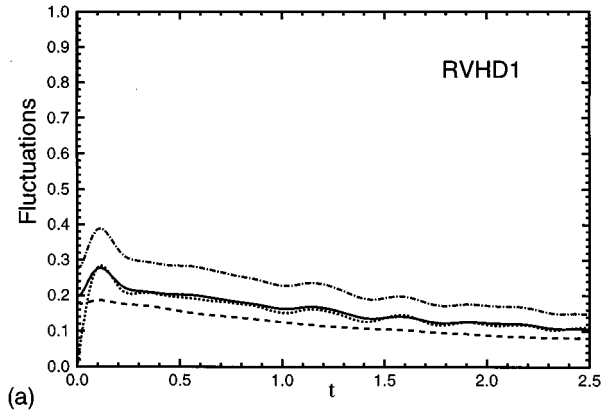
FIG. 7. Time evolution of rms density, ρ'_{rms}, temperature, T'_{rms}, pressure, p'_{rms} and $\gamma\rho'_{rms}$ in (a) case RVHD1 ($\chi_0=0.6$, $M_{t0}=0.3$); (b) case RVHD2 ($\chi_0=0.6$, $M_{t0}=0.5$); (c) case RVHD3 ($\chi_0=0.6$, $M_{t0}=0.7$):—, ρ'_{rms}; ---, T'_{rms}; $\cdots$, p'_{rms}; ---, $\gamma\rho'_{rms}$.

FIG. 8. Time evolution of rms density, ρ'_{rms}, temperature, T'_{rms}, pressure, p'_{rms} and $\gamma\rho'_{rms}$ in (a) case LVHD1 ($\chi_0=1$, $M_{t0}=0.3$); (b) case LVHD2 ($\chi_0=1$, $M_{t0}=0.5$); (c) case LVHD3 ($\chi_0=1$, $M_{t0}=0.7$):—, ρ'_{rms}; ---, T'_{rms}; $\cdots$, p'_{rms}; ---, $\gamma\rho'_{rms}$.

8(c), the results for LVHD3 show the same kind of affinity to those of RVHD3 [Fig. 7(c)]. $T'_{rms}<\rho'_{rms}<p'_{rms}\simeq\gamma\rho'_{rms}$, in both cases, but the enhancement of the amplitudes of these fluctuations in the LVHD case is about 30% over those in the RVHD simulation. It should be noted that when $p'_{rms}=\gamma\rho'_{rms}$, the amplitudes of pressure and density fluctuations are sufficiently large that Eq. (2) is no longer valid.

In Table II, columns 6, 7 and 8, we present, for each of the eight simulation cases, the ratio of the magnitude of in-compressible to compressible pressure fluctuations, $R_p=|p'^I_{rms}/p'^C_{rms}|$, the density–pressure correlation coefficient $C_{\rho p}=\langle\rho'p'\rangle/\rho'_{rms}p'_{rms}$, and the density–temperature correlation coefficient $C_{\rho T}=\langle\rho'T'\rangle/\rho'_{rms}T'_{rms}$ at 2.5 eddy turn over times of evolution. Initially, for all cases, by the process in which initial conditions were set (see Sec. III): $R_p(0)=1$; $C_{\rho p}(0)=0$; $C_{\rho T}(0)=-1$. The choice of $t=2.5$ is arbitrary, since, beyond the initial transient period, which is always less than $t=0.5$, each of these quantities is stable, with small oscillations or slow decay.
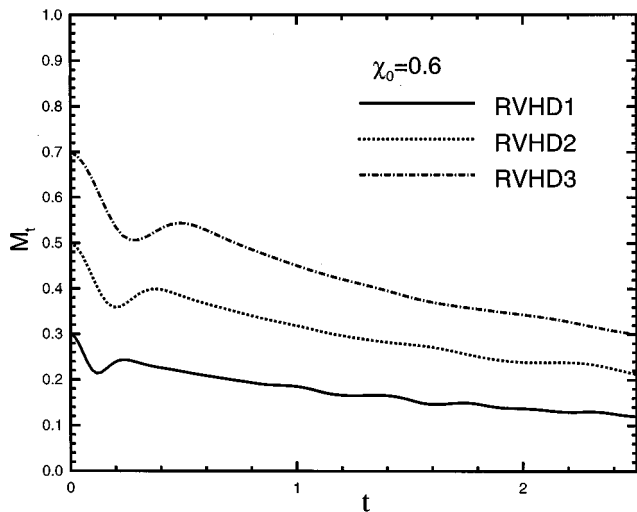
FIG. 9. Time evolution of turbulent Mach number, M_t, with initial energy ratio, $\chi_0 = 0.6$.—, $M_{t0} = 0.3$; $\cdots$, $M_{t0} = 0.5$; ---, $M_{t0} = 0.7$.

Again, it is clear from Table II that only the SVHD1 case can be considered to approximate the thermodynamic scalings based on NI hydrodynamic theory in which $C_{\rho\rho} \simeq 0$, $C_{\rho T} \simeq -1.0$, and the exchange between compressible and incompressible energy is weak, $R_p \simeq 1$. When M_{t0} is increased from 0.3 to 0.5 (SVHD2) there is a significant divergence from NI predictions. In the three RVHD cases, and the three LVHD cases, there is a monotonic increase of R_p with M_{t0} when χ_0 is fixed. This result, the increase in size of incompressible pressure fluctuations over those of compressible pressure fluctuations as the Mach number is increased, was at first surprising, but it is in fact consistent with Eq. (3), whereby $p'^C = \bigcirc(M_t)$, and the scaling result for incompressible pressure $p'^I = \bigcirc(M_t^2)$. In the SVHD cases R_p increases less noticeably with Mach number. This is apparently caused by the fact that $\chi_0 \simeq 0$ in these cases. It can be seen from Table II, column 4, that $\chi(t)$ at $t \simeq 2.5$ is about 3 times as large for SVHD2 as for SVHD1. Conse-

quently a more careful estimate $p'^C = \bigcirc(M_t \chi^{1/2})$ and $p'^I = \bigcirc[M_t^2(1 - \chi)]$ shows that $R_p \simeq \bigcirc(M_t/\chi^{1/2})$, may change only marginally when M_{t0} increases from 0.3 to 0.5 if $\chi \ll 1$ and has the behavior shown in column 4.
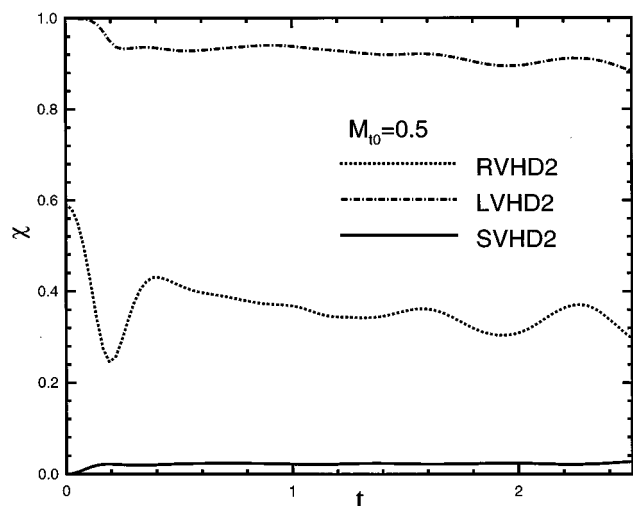
Except at the lowest Mach number, $M_{t0} = 0.3$, density and temperature fluctuations are weakly correlated for both RVHD and LVHD simulations, whereas density and pressure become even more closely correlated as the Mach number is increased, until the acoustic limit $p' \simeq \gamma \rho'$ is approached. On the other hand it is clear from Table II that the values of $C_{\rho\rho}$ vary little between RVHD and LVHD cases with the same initial Mach number. These seems to be a kind of saturation so that the effect of χ_0 on $C_{\rho\rho}$ is no greater at $\chi_0 \simeq 1$ than at $\chi_0 = 0.6$. The relatively large pressure fluctuations and strong correlation between density and pressure at high compressibility suggest that pressure fluctuations play a more important role than previously thought.[4] The increase of $C_{\rho T}$ from negative to slightly positive as M_{t0} is increased to 0.7 is consistent with experimental and simulational observations[19] of a slightly positive density–temperature correlation well away from the wall in a high Mach number flow.

Figures 9 and 10, respectively, show typical results for the evolutions of $M_t(t)$ with χ_0 fixed, and $\chi(t)$ with M_{t0} fixed. The values of χ and M_t at the particular time $t = 2.5$ are also displayed in column 4 and 5, respectively, of Table II. $M_t(t)$, for the RVHD cases with $\chi_0 = 0.6$, is presented in Fig. 9. The decay of $M_t(t)$ is monotonic in all three cases (except for some small oscillations in RVHD1), if the initial transient from NI scaling is excluded. RVHD3, which had the highest initial Mach number decays more rapidly than RVHD2, which itself decays somewhat faster than RVHD1. The dependence of M_t on χ_0 appears to behave predictably in these cases, and for all the other simulations not shown. The behavior of $\chi(t)$ with M_{t0} fixed is displayed in Fig. 10, using the three cases for which $M_{t0} = 0.5$. $\chi(t)$ decreases moderately and smoothly with time (beyond the initial transient) in case LVHD2, and moderately but in a somewhat more oscillatory mode in case RVHD2. $\chi(t)$ increases monotonically with time but remains at a low level for SVHD2, in which $\chi_0 = 0$; this behavior causes the weak dependence of R_p on M_{t0} in SVHD cases, as explained in a previous paragraph. The source of oscillation in $\chi(t)$ for the RVHD cases is not clear.

The two simulations mentioned at the beginning of this section as not appearing in the figures or tables, were SVHD cases ($M_{t0} = 0.3$ and 0.5) for which we varied the initial condition on pressure fluctuations by forcing the initial compressible pressure to be zero. Although the initial transients were quite different from those presented in Fig. 6 there was no discernible difference in the long term thermodynamic rms or correlation data shown on those figures, or in Table II.

V. CONCLUSIONS

The SVHD1 simulation has reproduced, approximately, the NI thermodynamic scalings predicted by Zank and Matthaeus.[8] Except for simulation SVHD1 it is clear that NI based scalings for the thermodynamic quantities, pressure,

FIG. 10. Time evolution of energy ratio, χ_0, with initial turbulent Mach number, $M_{t0} = 0.5$.—, $\chi_0 = 0$; $\cdots$, $\chi_0 = 0.6$; ---, $\chi_0 = 1.0$.

Cai, O'Brien, and Ladeinde

density and temperature are not adequate descriptions of compressible turbulence with large initial temperature variations and the pressure fluctuations do not remain small compared to the mean when the energy ratio or the Mach number is increased. This is consistent with similar behavioral results for RV and LV in isothermal cases.[5] The thermodynamic behavior in regimes in which NI scalings do not apply, has been presented for situations in which the initial temperature fluctuations are large compared to the initial pressure fluctuation and for turbulent Mach numbers up to 0.7. Fluctuations of, and correlations between, temperature, pressure and density are strong functions of both initial turbulent Mach number M_{t0} and initial energy ratio χ_0, but they are monotonic and stable functions which seem to approach a kind of saturation of their relative values when $M_{t0} > 0.5$ and $\chi_0 \geq 0.6$.

The asymptotic state of acoustic turbulence, in which $p' = \gamma \rho'$, is approximately attained when $M_{t0} = 0.7$ and $\chi_0 = 1.0$, and, in that state, density and temperature are effectively uncorrelated at two eddy turnover times, despite being perfectly anti-correlated initially.

Equation (3), an equation for function F, introduced in a simple context, is, on average, a very accurate predictor of the relationship between compressible pressure fluctuations, turbulent Mach number and energy ratio for all the cases we have computed. We have no definitive explanation for this behavior at present. The same conclusion also holds for the two cases we computed, but have not shown, which had different initial conditions than those listed in Table II.

ACKNOWLEDGMENTS

[1] P. A. Libby and F. A. Williams, *Turbulent Reacting Flows* (Springer-Verlag, 1994), Part 1, p. 8.

[2] S. Sarkar, ''The pressure–dilatation correlation in compressible flows,'' Phys. Fluids A **4**, 2674 (1992).

[3] S. Sarkar, G. Erlebacher, M. Y. Hussaini, and H. O. Kreiss, ''The anaysis and modelling of dilatational terms in compressible turbulence,'' J. Fluid Mech. **227**, 473 (1991).

[4] M. V. Morkovin, ''Effects of compressibility on turbulent flows,'' in *Mecanique de la Turbulence,* edited by A. Favre, CNRS, Paris (1961), pp. 367–80.

[5] S. Ghosh and W. H. Matthaeus, ''Low Mach number two-dimensional hydrodynamic turbulence: Energy budgets and density fluctuations in a polytropic fluid,'' Phys. Fluids A **4**, 148 (1991).

[6] T. Passot and A. Pouquet, ''Numerical simulation of compressible homogeneous flows in the turbulent regime,'' J. Fluid Mech. **181**, 441 (1987).

[7] G. P. Zank and W. H. Matthaeus, ''Nearly incompressible hydrodynamics and heat conduction,'' Phys. Rev. Lett. **64**, 1243 (1990).

[8] G. P. Zank and W. H. Matthaeus, ''The equations of nearly incompressible fluids. I. Hydrodynamics, turbulence, and waves,'' Phys. Fluids A **3**, 69 (1991).

[9] B. J. Bayly, C. D Levermore, and T. Passot, ''Density variations in weakly compressible flows,'' Phys. Fluids A **4**, 945 (1992).

[10] S. Klainerman and A. Majda, ''Compressible and incompressible fluids,'' Commun. Pure Appl. Math. **35**, 629 (1982).

[11] S. Kida and S. A. Orszag, ''Energy and spectral dynamics in decaying compressible turbulence,'' J. Sci. Comput. **7**, 1 (1992).

[12] G. Erlebacher, M. Y. Hussaini, H. O. Kreis, and S. Sarkar, ''The analysis and simulation of compressible turbulence,'' Theor. Comput. Fluid Dyn. **2**, 73 (1990).

[13] C.-W. Shu, T. A. Zang, G. Erlebacher, D. Whitaker, and S. Osher, ''High-order ENO schemes applied to two- and three-dimensional compressible flow,'' ICASE Report No. 91-38, 1991; also J. Appl. Num. Math. **9**, 45 (1992).

[14] G. K. Batchelor, *The Theory of Homogeneous Turbulence* (Cambridge University Press, Cambridge, 1956).

[15] F. Ladeinde, E. E. O'Brien, and X. D. Cai, ''A parallelized ENO procedure for direct numerical simulation of compressible turbulence,'' J. Sci. Comput. **11**, 179 (1996).

[16] F. Ladeinde, E. E. O'Brien, X. D. Cai, and W. Liu, ''Advection by polytropic compressible turbulence,'' Phys. Fluids **7**, 2848 (1995).

[17] D. H. Porter, A. Pouquet, and P. R. Woodward, ''Kolmogorov-like spectra in decaying three-dimensional supersonic flows,'' Phys. Fluids **6**, 2133 (1994).

[18] J. E. Moyal, ''The spectra of turbulence in a compressible fluid: Eddy turbulence and random noise,'' Math. Proc. Cambridge Philos. Soc. **48**, 329 (1952).

[19] G. N. Coleman, J. Kim, and R. D. Moser, ''A numerical study of turbulent supersonic isothermal-wall channel flow,'' J. Fluid Mech. **305**, 159 (1995).